PCCP

Accepted Manuscript

This is an *Accepted Manuscript*, which has been through the Royal Society of Chemistry peer review process and has been accepted for publication.

Accepted Manuscripts are published online shortly after acceptance, before technical editing, formatting and proof reading. Using this free service, authors can make their results available to the community, in citable form, before we publish the edited article. We will replace this *Accepted Manuscript* with the edited and formatted *Advance Article* as soon as it is available.

You can find more information about *Accepted Manuscripts* in the Information for Authors.

Please note that technical editing may introduce minor changes to the text and/or graphics, which may alter content. The journal's standard Terms & Conditions and the Ethical guidelines still apply. In no event shall the Royal Society of Chemistry be held responsible for any errors or omissions in this *Accepted Manuscript* or any consequences arising from the use of any information it contains.

ROYAL SOCIETY OF CHEMISTRY

www.rsc.org/pccp

Physical Chemistry Chemical Physics

ARTICLE TYPE

Cite this: DOI: 10.1039/c0xx00000x

www.rsc.org/xxxxxx

Elucidating the real-time Ag nanoparticle growth on α-Ag_2WO_4 during electron beam irradiation: Experimental evidence and theoretical insights

Wyllamanney da Silva Pereira,[a] Juan Andrés,*[b] Lourdes Gracia,[b] Miguel A. San-Miguel,[c] Edison Z. da Silva,[d] Elson Longo,[e] and Valeria M. Longo[f]

Received (in XXX, XXX) Xth XXXXXXXXX 20XX, Accepted Xth XXXXXXXXX 20XX
DOI: 10.1039/b000000x

Why and how Ag is formed when electron beam irradiation takes place on α-Ag_2WO_4 in a vacuum transmission electron microscopy chamber? To find an answer, the atomic-scale mechanisms underlying the formation and growth of Ag on α-Ag_2WO_4 have been investigated by detailed *in situ* by transmission electron microscopy (TEM) and by field emission scanning electron microscopy (FE-SEM) studies, density functional theory based calculations and *ab initio* molecular dynamics simulations. The growth process at different times, chemical composition, size distribution and the element distribution were analyzed in depth at the nanoscale level using FE-SEM, operated at different voltages (5, 10, 15, and 20 kV) and TEM with energy dispersive spectroscopy (EDS) characterization. The Ag nanoparticle sizes cover a wide range of values. Most of the Ag particles are in the 20-40 nm range. The Ag nucleation and formation on α-Ag_2WO_4 is a result of structural and electronic changes of the AgO_x (x=2,4, 6, and 7) clusters as a constituent building block of this material, consistent with Ag metallic formation. First principle calculations point out that Ag-3 and Ag-4-fold coordinated centers, located in the sub-surface of the (100) surface, are the most energetically favorable to undergo the diffusion process to form metallic Ag. *Ab initio* molecular dynamics simulations and the nudged elastic band (NEB) method were used to investigate the minimum energy pathways of these Ag atoms from positions in the first slab layer to outward sites on the (100) surface of α-Ag_2WO_4. The results point out that the injection of electrons decreases the activation barrier for this diffusion step and this unusual behavior results from the presence of a lower energy barrier process.

1. Introduction

An important branch of modern science is devoted to the study of a quantum phenomenon associated with the interaction of electron irradiation and electromagnetic radiation with matter. Predicting the response of a material to the passage of electrons and waves, respectively, is a very challenging problem. The understanding of spatial scales of atoms and chemical bonds and on temporal scales of electron and nuclear motion has gained increasing sophistication through development of precise photon and electron probes. The physical and chemical properties of a material are determined by the type of motion its electrons are allowed to execute. Therefore, the ultimate goal is to resolve the fundamental temporal and spatial scales of electron and nuclear motion.

A free electron exerts a force onto a nanostructure as it approaches. At long distances this is primarily a Coulomb type interaction but when the electron enters the region of charge density it becomes indistinguishable from the nanomaterial electrons so that additional quantum mechanical exchange interactions become effective. The irradiation of electrons induces the presence of hot (unbound or unconfined) electrons that are not quantized and can thus absorb any amount of energy, modifying the physical and chemical properties of the material. Despite of the importance of this phenomenon, the fundamental physical picture is still unclear, and an understanding of the electronic rearrangement processes is mandatory.

Transmission electron microscopy (TEM) and field emission scanning electron microscopy (FE-SEM) are well recognized techniques that provide unique capabilities for *in situ* imaging and control of nanoscale phenomena.[1-5] They provide, at the same time, morphological and crystallographic information such as the size and shape of the nanoparticles, the crystallographic phase, the arrangement of atoms in the specimen, and their degree of order.[6-9] The effects introduced with an electron beam in a TEM are directly analyzed from the produced TEM images, and the analysis on the scattering the electrons that exit the specimen back surface provides much microstructure/electronic structure

Physical Chemistry Chemical Physics Accepted Manuscript

information on the samples based on a variety of electron–solid interaction mechanisms. Therefore, direct observation of the structures is a powerful scientific tool in the material sciences and provides dynamic information on the solid surface, which cannot be obtained directly by other *in situ* techniques.[7]

Different research groups have utilized the electron beam to promote the chemical precipitation of nanoparticles from solution, [2,10-12] and to induce the deposition of metals and semiconductors from various precursor.[13-15] The role of the electron beam in affecting the chemical reactions have been analyzed.[2,16] A wide variety of metal nanoparticles with different morphologies have also been synthesized and characterized via electron microscopy.[17-25] Some reviews of these syntheses and related processes involving electron energy loss experiments have been published.[26,27] In these studies an electron beam is used for structural and morphological characterization, and can be used to carry out dynamic *in situ* experiments.[28] In particular, the development of liquid cells for TEM has enabled dynamic information about nanosystems and direct observation of nanoparticle growth in a liquid phase.[1,29,30]

The effect *in vacuo* is quite different since the liquids have a strong influence on their physical and chemical properties. During imaging, the electron beam interacts with the sample, and different research groups have reported nanoscale crystallization and growth processes taking place only in the beam's presence.[2,10,12,16,30-32] Specifically, plasmonic noble metal nanocrystals have recently been found to enhance a number of chemical reactions due to localized surface plasmon resonances.[33-45] However, the nature of the mechanism of the plasmonic driven chemistry with presence of hot electrons or charged species and concurrent photoluminescence properties over plasmonic particles are not well understood.[33,37,46,47]

This investigation's motivation essentially arises from a discovery of an unwanted real-time *in situ* nucleation and growth of Ag filaments on α-Ag_2WO_4 crystals which was driven by an accelerated electron beam from an electronic microscope under high vacuum.[48,49] This is the first example of such studies in the scientific literature and it has become a major topic in current research. It is a novel example of dynamic single crystals where electron irradiation induces macroscopic mobility presenting a visually appealing demonstration of their potential for bactericide and photoluminescent applications,[50,51] as well their application as an efficient ozone sensor have been reported.[52] But, they also provide a unique opportunity to explore the mechanistic link between collective atomic processes and their consequences at a macroscopic level. This phenomenon is of an electron-driven nature. The key difference in this approach is the use of an electron beam of TEM for growing Ag nanoparticles rather than for optical or electromagnetic erasing as is the case in the plasmon effect. Knowledge of the driving force and origin of this phenomenon is of utmost importance.

An electron beam was used to grow Ag nanoparticles from α-Ag_2WO_4 crystals. TEM and field emission scanning electron microscopy (FE-SEM) were used to study these materials. The growth process (at different times), chemical composition, size distribution and element distribution were analyzed in depth at the nanoscale level using FE-SEM, operated at different voltages (5, 10, 15, and 20 kV) and TEM with energy dispersive spectroscopy (EDS) characterization. First principle calculations are essential in understanding the experimental observations and for gaining a more complete understanding of this intricate mechanism at atomic levels. First principles density functional theory (DFT) calculations have been carried out to obtain a better understanding of the processes that occur during the initial stages of Ag nanoparticle formation. This present work can be considered a combination of experimental and theoretical studies based on the results obtained by experimental techniques and calculations carried out by the DFT method in order to provide a deeper understanding of atomic and electronic structures associated with the formation of Ag, which was followed by a subsequent nano- to micro-scale growth process.

The research discussed in the present study provides a convenient example of a "complex modeling paradigm", as was introduced by Billinge and and Levin[53] as an appropriate procedure for combining the results of multiple experimental methods and theory in a self-consistent computational framework leading to a greater understanding of this process. Four sections complete this article. The experimental procedure details are presented in section 2. The computational details are given in section 3. In Section 4, experimental and theoretical results are presented and discussed in detail. A brief summary and the main conclusions will be offered in the final section.

2. Experimental procedure

Synthesis of α-Ag_2WO_4

α-Ag_2WO_4 microcrystals were prepared at 358K for 30 min by a simple precipitation method without the use of any surfactant. The typical α-Ag_2WO_4 crystals synthesis procedure is described as follows: 1×10^{-3} mol of tungstate sodium dihydrate ($Na_2WO_4.2H_2O$; 99.5% purity, Sigma-Aldrich) was dissolved in 5 ml deionized water and 2×10^{-3} mols of silver nitrate ($AgNO_3$; 99.8% purity, Sigma-Aldrich) were dissolved in 95 mL of deionized water at 358K. The tungstate solution was added to the silver solution with stirring. The resulting suspensions were washed with deionized water and acetone several times to remove remaining ions and dried at 60ºC for 12 h.

Experimental characterizations of α-Ag_2WO_4

The α-Ag_2WO_4 crystals were structurally characterized by X-ray diffraction (XRD) patterns using a diffractometer model LabX XRD-6000 (Shimadzu®, Japan) with Cu-Kα radiation (λ = 1.5406 Å) in the 2θ range from 10° to 70° with a scanning velocity of 1°/min. The shapes, sizes, visualization of Ag filaments and element distribution of the α-Ag_2WO_4 microcrystals were observed with a FEG-SEM model Supra 35-VP, Carl Zeiss, Germany operated at 5, 10, 15 and 20 kV, and TEM operating at 200 KV, and EDS; model Tecnai G2TF20, FEI.

3. Computational details

Periodic DFT based calculations were performed using the VASP code.[54-56] The valence electrons are described with a plane wave basis set and the effect of the inner cores on the valence electron density is taken into account using the projector augmented wave (PAW) method.[57,58] The valence states that are explicitly included in the calculation are *5d* and *6s* (6 electrons) for W, *4d* and *5s* (11 electrons) for Ag atoms, and *2s* and *2p* (6 electrons) for O atoms. The rest of the electrons are considered as core electrons and their densities are kept frozen as in the reference used to extract the PAW potential. A kinetic energy cutoff of 460 eV for the plane wave expansion is used for all systems, which is adequate to obtain total energies converged to at least 1 meV/atom.

The Brillouin zone was sampled using the Monkhorst–Pack method and at different *k*-points grids according to the system size. The number of k-points was increased for the analysis of the electronic structure with respect to the geometry optimization process and the tetrahedron method with Blöchl corrections[59] was

Physical Chemistry Chemical Physics Accepted Manuscript

This journal is © The Royal Society of Chemistry [year]

also used. All calculations were non spin-polarized. The generalized gradient approximation (GGA) in the Perdew–Burke–Ernzerhof (PBE) formulation was used for the electron exchange and correlation contribution to the total energy.[60, 61] The conjugated gradient (CG) energy minimization method was used to obtain relaxed systems. Atoms are considered to be are fully relaxed when the Hellmann−Feynman forces converged to less than 0.005 eV/Å per atom.

Ab initio molecular dynamics simulations were performed in selective cases in the canonical ensemble at 300 K. The time step was 3 fs, and a typical simulation spanned about 3 ps. The Nudged Elastic Band (NEB) method was used to investigate the minimum energy pathways of the Ag atoms from positions in the first slab layer to outward sites on the nanoparticle surface. Both the initial and end point configurations were previously optimized. Then intermediate configurations were generated by linear interpolation between the initial and end points. Finally, the intermediate configurations were relaxed under the constraint that the ions were connected by springs to keep them equidistant from neighboring configurations. Details of the NEB method are described by Jonsson et al.[62]

4. Results and discussion

Fig. 1 shows the XRD patterns. All of the diffraction peaks of samples can be can be assigned to the orthorhombic α-Ag_2WO_4 with a space group Pn2n (JCPDS card No.4165), and the strong diffraction peaks revealed crystallinity. The sample was totally monophased α-Ag_2WO_4, in good agreement with previous observations in neutral[63-66] or slightly alkaline[67] media. In α-Ag_2WO_4 crystals, Ag ions can display different AgOx clusters corresponding to type-coordination and synergistic coordination modes in order to facilitate the formation of several clusters with low and high coordination numbers (x = 2, 4, 6 and 7).

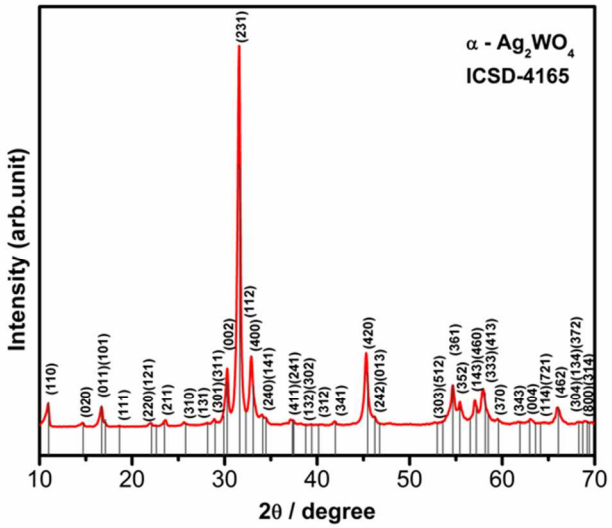

Fig. 1 XRD of an α−Ag_2WO_4 sample.

The TEM image in Fig. 2 clearly demonstrates the formation of Ag nanoparticles on α-Ag_2WO_4 microrods at different times (from 0 to 5 minutes). Some nanoparticles assemble into flower-like aggregates. The rod surface is observed to be smooth.

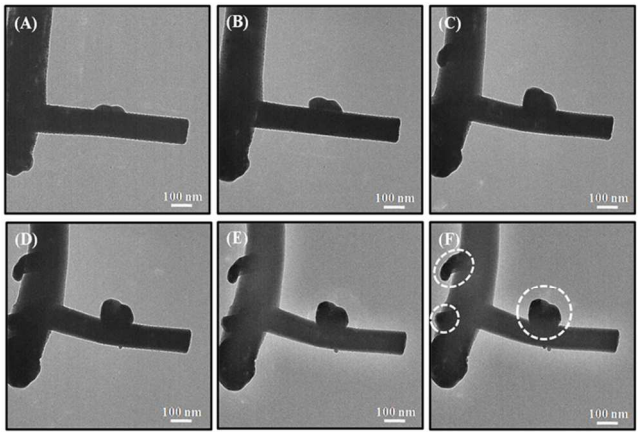

Fig. 2 TEM images of a α−Ag_2WO_4 sample obtained at (A) time zero, (B) 1 min, (C) 2 min, (D) 3 min, (E) 4 min and (F) 5 min of exposure to electron beam. Ag nanoparticles appear in the middle of both microrods.

Fig. 3 (A-H) shows a FE-SEM image of the crystals that were obtained after a rapid approach and focus adjustment (time zero) at 5, 10, 15 and 20 kV, during the growth of Ag when stimulated by the electron beam on the α-Ag_2WO_4 surface. Further information on the Ag growth process can be found in the Supplementary Information.

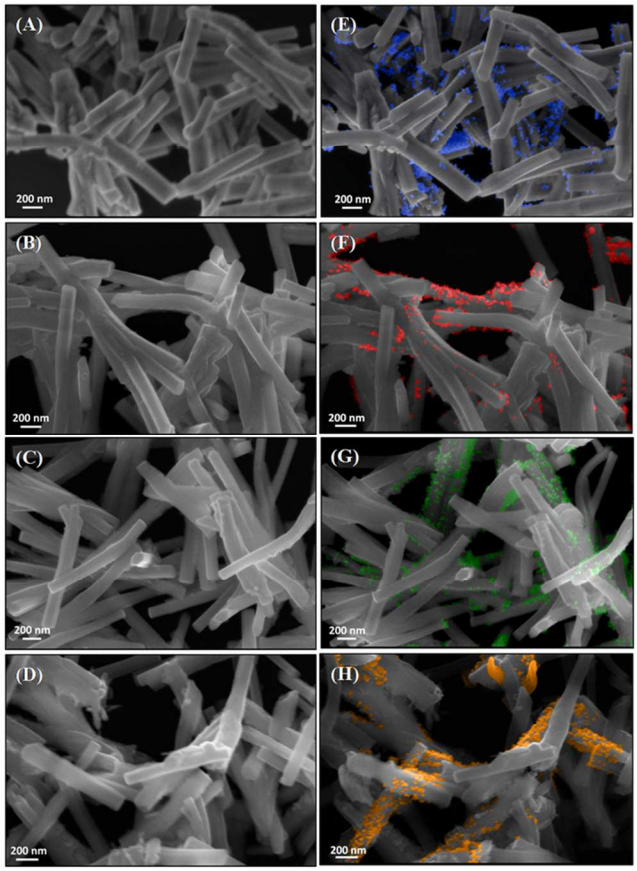

Fig. 3 Time-resolved FE-SEM images of α−Ag_2WO_4 operated at different voltages (A - E) 5 kV, (B - F) 10 kV, (C - G) 15 kV, (D - H) 20 kV. A, B, C and D images were obtained at zero time while E, F, G and H images are displayed after 5 min of exposure to the electron beam.

Physical Chemistry Chemical Physics Accepted Manuscript

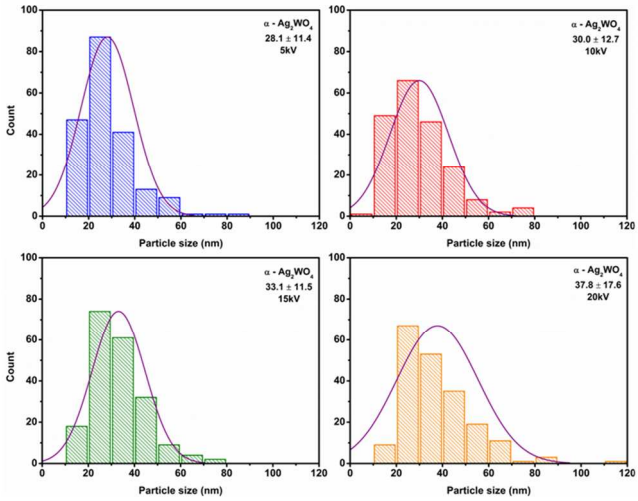

Fig. 4 Mean particle diameter distribution at 5 minutes of electron beam exposure for different voltages. Violet curves are normal fits.

This phenomenon occurs after a few seconds of exposure. An analysis of the images reveals increasing formation of Ag nanoparticles on the surface with increasing voltage. The size distribution of the Ag nanoparticles at different voltages for 5 minutes has been obtained and the results are displayed in Fig. 4. Different configurations can be formed during the rapid growth of Ag nanoparticles generating Ag vacancies defects, which can be responsible for the different average particle size distributions. An analysis of the results shows two important facts. The first is related to the distribution range that increases with the increasing time and the second is that the nanoparticles size increases with increasing voltage.

In this typical semiconductor, the electronic structure of the α-Ag_2WO_4 microcrystal is governed by both inter cluster (intermediary range) and intra-cluster (local range) of the cluster constituents of this material: AgO_2, AgO_4, AgO_6, and AgO_7, and the electron-hole pairs are produced in these clusters. When the electrons hit the surface, the oxidation of stoichiometric Ag_2WO_4 into non-stoichiometric $Ag_{2-x}WO_4$ can accelerate the generation of LSPRs.[68, 69] All of these LSPRs are based on the tunable hole concentration induced by the Ag vacancies in Ag_2WO_4 surface. This perspective addresses the exciting fundamental opportunities arising from the plasmon resonances of semiconductors. The LSPR can be considered, in the most general sense, as an optical signature of any arbitrary collection of charge carriers. It is not essential for the arbitrary collection of charge carriers. It is not essential for these charges to have purely free character.[20, 70-72]

Fig. 5 illustrates the TEM images with EDS characterization. Composition results are shown in Table 1. Therefore the end of the region that emerged due to the electron exposure (point 1) confirmed the composition of 100% of Ag in relation to W. It is possible to see the crystallographic planes revealing the Ag crystallinity. The region near the interface, point 2, is composed of about 92.5% of Ag to 7.5% of W; while, for the internal region, point 3, shows 96.9% of W. These results reinforce the fact that the Ag atoms come from the interior deep regions of the particles. This behavior induces the presence of Ag defects inside α-Ag_2WO_4 material and this semiconductor changes from an *n* to a *p* type.

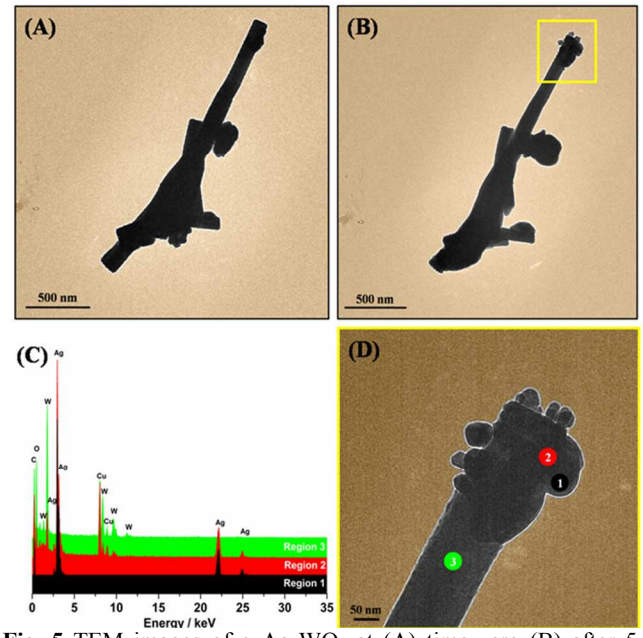

Fig. 5 TEM images of α-Ag_2WO_4 at (A) time zero (B) after 5 minutes of exposure. (C) EDS spectra for the three regions, corresponding to points 1, 2 and 3, respectively, are depicted in (D)

Table 1 Ag and W relationship shown by EDS.

Points	Ag (%)	W (%)
1	100	0
2	92.50	7.49
3	3.1	96.9

Adsorption and absorption of electrons by the semiconductor Ag_2WO_4 followed by removal of silver causes distortion and breaking of the crystal symmetry. This physico-chemical effect produces the polarization between the clusters that makes the population of electronic excited states easy. These electrons reduce $[AgO_x]$ $[V'_{Ag}.O_x]$ and Ag^o, but are not energetic enough to reduce $[WO_6]^x$ clusters. The cluster-to-cluster charge transfer in α-$Ag_{2-x}WO_4$ crystal containing more than one kind of cluster is characterized by excitations involving electronic transitions from on cluster to another cluster. Therefore, these clusters have favorable conditions to promote the charge transfer process from $[V'_{Ag}.O_x]$ clusters to $[AgO_x]$ clusters. This electronic transition between clusters probably occurs when α-$Ag_{2-x}WO_4$ microcrystals with distorted clusters are able to absorb electrons with a quantum confinement effect associated with electron reduction of silver clusters.

Ag nanoparticles emerge from the structure of α-$Ag_{2-x}WO_4$ and xAg^o. Collective plasmon excitations provides a connection between the semiconductor and Ag nanoparticles resulting an increase of silver nanowire carriers, i.e. these emerging nanowires have a high defect density and the interactions at both intermediate and short ranges result in a dynamic equilibrium of formation of unstable clusters which leave the surface of the nanowire, forming clusters. This coupling semiconductor-metal-cluster opens the perspective of a new phenomenon of nature involving the effect of quantum confinement on plasmon resonance, i.e., an optical signature nanoscale produced by charge carriers.

Physical Chemistry Chemical Physics Accepted Manuscript

This journal is © The Royal Society of Chemistry [year]

Bulk calculations

The α-Ag_2WO_4 bulk structure was calculated under full structural relaxation, which allowed for changes in the lattice parameter and the internal atomic positions. The calculated cell parameters were a = 11.234 Å, b = 12.574 Å and c = 5.812 Å which compare well with experimental values.[45, 63] α-Ag_2WO_4 crystals belong to an orthorhombic structure with a space group of Pn2n, with a point-group $C_2v^{(10)}$ symmetry.[73] The bulk structure is formed by clusters of [WO_6] and [AgO_y] (y = 2, 4, 6 and 7).

The (100) surface

The difference between surface and bulk properties is linked to the role of dimensionality, and we have studied the (100) surface, which is the most stable one. This surface is modelled using supercells with surface parameters of 11.624 x 12.574 Å. In order to test the reproducibility of results with respect to the slab thickness, we chose two different slab sizes of 3 and 6 layers resulting in systems with 84 and 168 atoms, respectively. The vacuum distance in this direction was set to 14 Å, which is large enough to avoid the interaction between the surface and its images. Once the supercell was created, all further relaxation processes were carried out allowing for the internal atomic positions to relax without changing the lattice parameters.

When cleaving the crystal, the coordination number of the surface atoms changes from the bulk situation. Thus, the W atoms change to a tetrahedral coordination, whereas the Ag atoms are found with coordination numbers of 4 and 6. The presence of these under-coordinated atoms modifies the electronic structure and distinguishes the surface from their bulk counterparts because of the bond contraction and bond energy elevation induced by atomic under-coordination. *Ab initio* molecular dynamics simulations of both slab models show that this oxide surface made of under-coordinated Ag atoms is suitable to undergo delicate structural rearrangements even at ambient temperature. The optimization process for both slabs leads to structures with some slight differences (see Fig. 6). However, and more importantly, the coordination number of all Ag atoms is preserved in both models, and the structural environment of each Ag atom can be considered approximately equivalent in both models. There are eight surface Ag atoms, which are arranged in four different arrangements. Ag-1 and Ag-2 are the outmost external Ag atoms and are four-fold coordinated. Ag-3 and Ag-4 are also four-fold coordinated, but they are in more internal positions. The next Ag atoms are even further into the slab and they are all six-fold coordinated. Only the smallest supercell model was used for performing the calculations that are described next, because the use of the 6-layer model would be too computationally demanding.

The mechanism of surface Ag nucleation induced by the electron injection starts from the presence of Ag adatoms on the surface. These reduced adatoms diffuse from the bulk material when hit by the electron bombardment. Presumably, the outmost external atoms would be more easily removed and would initiate the process. Geometry optimization of the system was done when each Ag atom is displaced to higher z coordinate outside the surface. There are no stable situations for the Ag-01, Ag-02, Ag-05, Ag-06 atoms and they were put back to the original positions. Conversely, the system is energetically favored at 0.25 eV when Ag-03 and Ag-04 are in external sites. In a similar way, the system is stabilized at 0.52 eV when Ag-07 and Ag-08 move outward, but a considerable surface rearrangement occurs simultaneously. We have computed the energy barrier for the diffusion process of Ag-03 and Ag-04 by means of the NEB method.

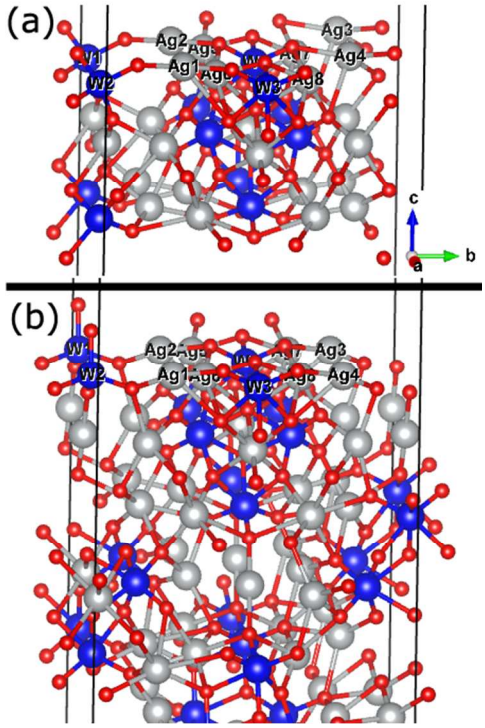

Fig. 6 Relaxed slab models for the (100) surface. (a) 3-layer and (b) 6-layer models.

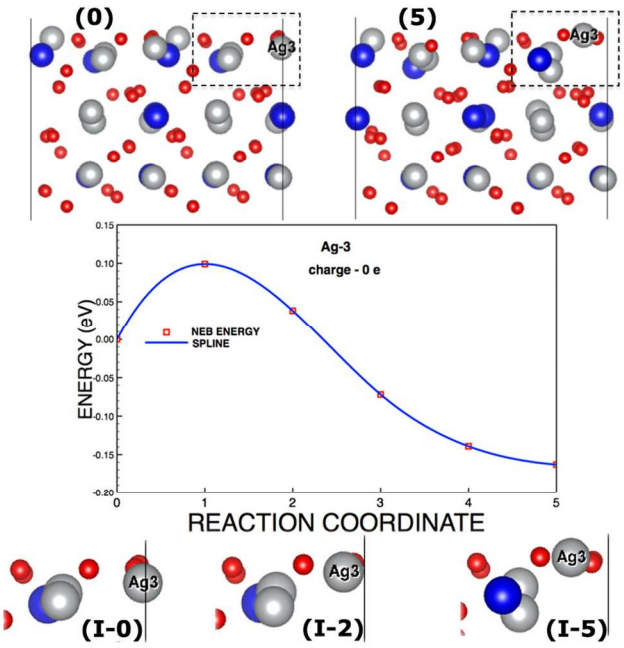

Fig. 7 Energy profile and structures obtained from a NEB calculation. The top two images labeled (0) and (5) are the initial and final structures, respectively. Insets of these structures and other intermediate along the reaction coordinate are labeled as (I-0), (I-5) and (I-2), respectively. The graph shows the energy profile along the reaction coordinate displaying a small barrier of 0.10 eV.

Fig. 7 shows the structures of the NEB evolution along the reaction coordinate (RC) from the initial position RC-00 (a) up to

Physical Chemistry Chemical Physics Accepted Manuscript

the final position RC-05 (f). Also, the energy profile along the reaction coordinate is depicted in the central plot. It corresponds basically to the movement of the Ag atom from the relaxed surface (RC-00) to the optimized situation when the atom is on the outer site (RC-05), which corresponds to a displacement of 0.65 Å. It can be seen that the energy cost is only around 0.10 eV, a low energy barrier, which makes this Ag surface atom very mobile and a good candidate to exit the surface and initiate the metal nucleation process.

Although these Ag-3 and Ag-4 surface atoms appear to be very mobile, the charge effect provided by the irradiation further helps this process. In order to verify this effect, the electron absorption process on the surface structure was also investigated. 1 to 3 electrons were added and relaxation of the surface clusters was analyzed Fig. 8 shows how the *z* coordinates of the surface Ag atoms change for each charge addition. It can be seen that as the number of injected electrons increases, the Ag-3 and Ag-4 atoms move outward whereas the positions of the other atoms do not significantly change.

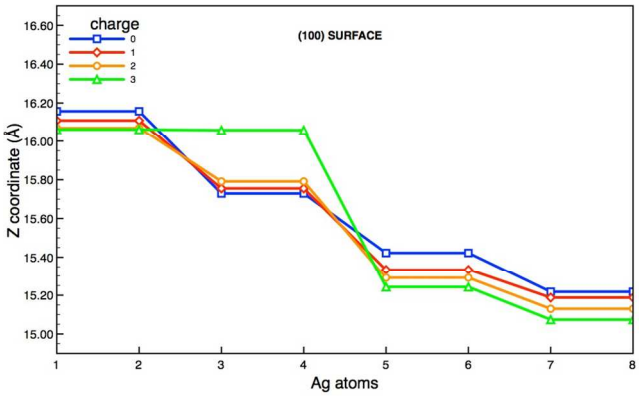

Fig. 8 *Z* coordinates of the surface Ag atoms for each charge addition.

This result indicates that electron excess favors Ag-3 and Ag-4 atoms to move to the outmost external sites. To confirm this behavior, NEB calculations have been used to estimate the energy barrier to diffusion for these atoms when one electron is added into the system. Figure 9 shows the diffusion energy profile and demonstrates that it is a non-barrier pathway. The small barrier presented (see Fig. 7) in the diffusion process (red squares) changes to a barrierless profile (red circles) with charging the system with one electron. Therefore these charge injection effects favor the escape of Ag atoms to form new Ag structures, nanowires and clusters as observed in the experiments presented in this article and in previous publications.[49-52]

5. Conclusions

In this study, α-Ag_2WO_4 samples were grown using a simple co-precipitation method. How the *in situ* Ag nanoparticle growth and morphological evolution on α-Ag_2WO_4 take place during electron beam irradiation has been analyzed. These events were directly monitored in real-time using *in situ* TEM and FE-SEM spectroscopic techniques and first principle calculations to provide a deeper insight and understanding of these processes in individual nanostructures at the atomic to nanoscale levels.

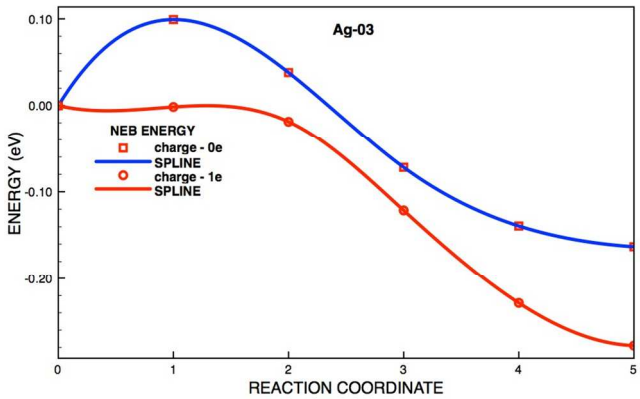

Fig. 9 Energy profiles for the diffusion process of the Ag-03 atom in a neutral system (blue line and red squares) and when one electron is added into the system (red circles).

This promising methodology was demonstrated based on the combination of experiments and calculations, through their application to a long-standing challenging problem, namely, the Ag nanoparticle growth and morphological evolution on α-Ag_2WO_4 during electron beam irradiation. The results of the present study can be summarized as follow: i) the formation of Ag nanoparticles takes place on the α-Ag_2WO_4 surface after a few seconds of exposure to an electron beam and is not dependent of the electron beam voltage. ii) the sizes of Ag nanoparticles covers a wide range of values, with most of the the Ag particles being 20-40 nm of size. iii) First principle calculations of the (100) surface, as most stable of α-Ag_2WO_4, allows a detailed analysis of the Ag active centers. iv) the theoretical results point out that Ag-3 and Ag-4 four-fold coordinated centers, located in the sub-surface, are the most energetically favorable to suffer the diffusion process to form metallic Ag. v) *Ab initio* molecular dynamics simulations and NEB calculations point out that the injection of electrons decreases the activation barrier for the diffusion process of these Ag centers.

The present study has drawn a fundamental physical picture for understanding electron-enhanced activity, and the data reveal real-time insights in the activation of α-Ag_2WO_4 by the electron beam and constitutes a new example of how and where silver nanoparticles are formed by modifying the electron density and opens the door to future transformations and applications.

Acknowledgements

The authors are grateful to Prometeo/2009/053 (GeneralitatValenciana), Ministerio de Economia y Competitividad (Spain), CTQ2012-36253-C03-02, Spanish Brazilian program (PHB2009-0065-PC), FAPESP (Project 2013/07296-2) (Project2012/14468-1) (Project 2010/16970-0), grant (2013/02032-7), CAPES and CNPq (Project 573636/2008-7, Grant 150753/2013-6) and CAPES (Project 088/2013) for financially supporting this research. Most of the calculations were performed using IFGW-UNICAMP computer facilities and the National Center for High Performance Computing in São Paulo (CENAPAD-SP). We also acknowledge the Servei Informática, Universitat Jaume I, for the generous allotment of computer time.

Physical Chemistry Chemical Physics Accepted Manuscript

This journal is © The Royal Society of Chemistry [year]

Notes and references

[a] *INCTMN-UFSCar, Universidade Federal de São Carlos, P.O. Box 676, 13565-905 São Carlos, SP, Brazil. E-mail: wyllamanneysp@gmail.com*
[b] *Departament de Química Física i Analítica, Universitat Jaume I (UJI), Castelló 12071, Spain. E-mail: andres@qfa.uji.es, lgracia@qfa.uji.es*
[c] *Institute of Chemistry - University of Campinas - Unicamp, 13083-970, Campinas, SP, Brazil. E-mail: smiguel@iqm.unicamp.br*
[d] *Institute of Physics "Gleb Wataghin", University of Campinas - Unicamp, 13083-970, Campinas, SP, Brazil. E-mail: zacarias@ifi.unicamp.br*
[e] *INCTMN-UNESP, Universidade Estadual Paulista, P.O. Box 355, CEP 14801-907 Araraquara, SP, Brazil. E-mail: elson.liec@gmail.com*
[f] *INCTMN-USP, Universidade de São Paulo, Instituto de Física de São Carlos, 13560-970 São Carlos, SP, Brazil. E-mail:lelalongo@icloud.com*

† Electronic Supplementary Information (ESI) available: [details of any supplementary information available should be included here]. See DOI: 10.1039/b000000x/

1. N. de Jonge and F. M. Ross, Nature Nanotechnology, 2011, 6 (11), 695-704.
2. T. J. Woehl, J. E. Evans, L. Arslan, W. D. Ristenpart and N. D. Browning, Acs Nano, 2012, **6** (10), 8599-8610.
3. R. F. Egerton, P. Li and M. Malac, Micron, 2004, **35** (6), 399-409.
4. L. R. Parent, D. B. Robinson, T. J. Woehl, W. D. Ristenpart, J. E. Evans, N. D. Browning and I. Arslan, Acs Nano, 2012, **6** (4), 3589-3596.
5. T. J. Woehl, K. L. Jungjohann, J. E. Evans, I. Arslan, W. D. Ristenpart and N. D. Browning, Ultramicroscopy, 2013, **127**, 53-63.
6. E. J. R. Vesseur, J. Aizpurua, T. Coenen, A. Reyes-Coronado, P. E. Batson and A. Polman, Mrs Bulletin, 2012, **37** (8), 752-760.
7. D. B. C. Williams, C. B., *Transmission Electron Microscopy: A Textbook for Materials Science*. (Springer, Berlin, 2009).
8. A. Yurtsever, M. Couillard and D. A. Muller, Physical Review Letters, 2008, **100** (21) 217402.
9. S. B. Simonsen, I. Chorkendorff, S. Dahl, M. Skoglundh, J. Sehested and S. Helveg, Journal of the American Chemical Society, 2010, **132** (23), 7968-7975.
10. J. E. Evans, K. L. Jungjohann, N. D. Browning and I. Arslan, Nano Letters, 2011, **11** (7), 2809-2813.
11. Y. Liu, K. Tai and S. J. Dillon, Chemistry of Materials, 2013, **25** (15), 2927-2933.
12. H. Zheng, R. K. Smith, Y.-w. Jun, C. Kisielowski, U. Dahmen and A. P. Alivisatos, Science, 2009, **324** (5932), 1309-1312.
13. E. U. Donev and J. T. Hastings, Nano Letters, 2009, **9** (7), 2715-2718.
14. Y. Liu, X. Chen, K. W. Noh and S. J. Dillon, Nanotechnology, 2012, **23** (38), 385302.
15. G. Schardein, E. U. Donev and J. T. Hastings, Nanotechnology, 2011, **22** (1), 015301.
16. K. W. Noh, Y. Liu, L. Sun and S. J. Dillon, Ultramicroscopy, 2012, **116**, 34-38.
17. S. E. Habas, H. Lee, V. Radmilovic, G. A. Somorjai and P. Yang, Nature Materials, 2007, **6** (9), 692-697.
18. F. Kim, S. Connor, H. Song, T. Kuykendall and P. D. Yang, Angewandte Chemie-International Edition, 2004, **43** (28), 3673-3677.
19. B. Lim, Y. Xiong and Y. Xia, Angewandte Chemie-International Edition, 2007, **46** (48), 9279-9282.
20. T. K. Sau and A. L. Rogach, Advanced Materials, 2010, **22** (16), 1781-1804.
21. D. Seo, C. I. Yoo, J. C. Park, S. M. Park, S. Ryu and H. Song, Angewandte Chemie-International Edition, 2008, **47** (4), 763-767.
22. A. R. Tao, S. Habas and P. Yang, Small **4** (3), 310-325 (2008).
23. N. Tian, Z.-Y. Zhou, S.-G. Sun, Y. Ding and Z. L. Wang, Science, 2007, **316** (5825), 732-735.
24. B. Wiley, Y. G. Sun, B. Mayers and Y. N. Xia, Chemistry-a European Journal, 2005, **11** (2), 454-463.
25. Q. Zhang, J. Xie, J. Yang and J. Y. Lee, Acs Nano, 2009, **3** (1), 139-148.
26. P. E. Batson, A. Reyes-Coronado, R. G. Barrera, A. Rivacoba, P. M. Echenique and J. Aizpurua, Nano Letters, 2011, **11** (8), 3388-3393.
27. F. J. Garcia de Abajo, Reviews of Modern Physics, 2010, **82** (1), 209-275.
28. S. W. Chee, S. Sivaramakrishnan, R. Sharma and J.-M. Zuo, Microscopy and Microanalysis, 2011, **17** (2), 274-278.
29. F. Tao and M. Salmeron, Science, 2011, **331** (6014), 171-174.
30. H.-G. Liao, K. Niu and H. Zheng, Chemical Communications, 2013, **49** (100), 11720-11727.
31. J. M. Yuk, J. Park, P. Ercius, K. Kim, D. J. Hellebusch, M. F. Crommie, J. Y. Lee, A. Zettl and A. P. Alivisatos, Science, 2012, **336** (6077), 61-64.
32. H. G. Liao, L. K. Cui, S. Whitelam and H. M. Zheng, Science, 2012, **336** (6084), 1011-1014.
33. P. Christopher, H. Xin and S. Linic, Nature Chemistry, 2011, **3** (6), 467-472.
34. S. Linic, P. Christopher and D. B. Ingram, Nature Materials, 2011, **10** (12), 911-921.
35. M. Xiao, R. Jiang, F. Wang, C. Fang, J. Wang and J. C. Yu, Journal of Materials Chemistry A, 2013, **1** (19), 5790-5805.
36. X. Zhang, Y. L. Chen, R.-S. Liu and D. P. Tsai, Reports on Progress in Physics, 2013, **76** (4).
37. W. H. Hung, M. Aykol, D. Valley, W. Hou and S. B. Cronin, Nano Letters **10** (4), 1314-1318.
38. D. B. Ingram and S. Linic, Journal of the American Chemical Society, 2010, **133** (14), 5202-5205 (2011).
39. S. Navalon, M. de Miguel, R. Martin, M. Alvaro and H. Garcia, Journal of the American Chemical Society, 2011, **133** (7), 2218-2226.
40. S.-i. Naya, A. Inoue and H. Tada, Journal of the American Chemical Society, 2010, **132** (18), 6292-+.
41. A. Primo, T. Marino, A. Corma, R. Molinari and H. Garcia, Journal of the American Chemical Society, 2011, **133** (18), 6930-6933.
42. E. Thimsen, F. Le Formal, M. Graetzel and S. C. Warren, Nano Letters, 2011, **11** (1), 35-43.
43. I. Thomann, B. A. Pinaud, Z. Chen, B. M. Clemens, T. F. Jaramillo and M. L. Brongersma, Nano Letters, 2011, **11** (8), 3440-3446.
44. D. Tsukamoto, Y. Shiraishi, Y. Sugano, S. Ichikawa, S. Tanaka and T. Hirai, Journal of the American Chemical Society, 2012, **134** (14), 6309-6315.
45. C. Gomes Silva, R. Juarez, T. Marino, R. Molinari and H. Garcia, Journal of the American Chemical Society, 2011, **133** (3), 595-602.
46. S. Mukherjee, F. Libisch, N. Large, O. Neumann, L. V. Brown, J. Cheng, J. B. Lassiter, E. A. Carter, P. Nordlander and N. J. Halas, Nano Letters, 2013, **13** (1), 240-247.
47. Z. Zhao and M. A. Carpenter, Journal of Physical Chemistry C, 2013, **117** (21), 11124-11132.
48. E. Longo, L. S. Cavalcante, D. P. Volanti, A. F. Gouveia, V. M. Longo, J. A. Varela, M. O. Orlandi and J. Andres, Scientific Reports, 2013, **3**, 1676.
49. J. Andrés, L. Gracia, P. Gonzalez-Navarrete, V. M. Longo, W. A. Jr, D. P. Volanti, M. M. Ferrer, P. S. Lemos, F. A. L. Porta, A. C. Hernandes and E. Longo, Scientific Reports, 2014, **5**, 5391.
50. E. Longo, D. P. Volanti, V. M. Longo, L. Gracia, I. C. Nogueira, M. A. P. Almeida, A. N. Pinheiro, M. M. Ferrer, L. S. Cavalcante and J. Andrés, The Journal of Physical Chemistry C, 2014, **118**, 1229–1239.
51. V. M. Longo, C. C. D. Foggi, M. M. Ferrer, A. F. Gouveia, R. S. André, W. Avansi, C. E. Vergani, A. L. Machado, J. Andrés, L. S. Cavalcante, A. C. Hernandes and E. Longo, J. Phys. Chem. A, 2014, **118**, 5769–5778.
52. L. F. da Silva, A. C. Catto, W. Avansi, Jr., L. S. Cavalcante, J. Andres, K. Aguir, V. R. Mastelaro and E. Longo, Nanoscale, 2014, **6** (8), 4058-4062.
53. S. J. L. Billinge and I. Levin, Science, 2007, **316** (5824), 561-565.
54. G. Kresse and J. Furthmuller, Computational Materials Science, 2007, **6** (1), 15-50.
55. G. Kresse and J. Furthmuller, Physical Review B, 1996, **54** (16), 11169-11186.
56. G. Kresse and J. Hafner, Physical Review B **47** (1), 558-561 (1993).

Physical Chemistry Chemical Physics Accepted Manuscript

57. P. E. Blochl, Physical Review B, 1994, **50** (24), 17953-17979.
58. G. Kresse and D. Joubert, Physical Review B, 1999, **59** (3), 1758-1775.
59. P. E. Blochl, O. Jepsen and O. K. Andersen, Physical Review B, 1994, **49** (23), 16223-16233.
60. J. P. Perdew, K. Burke and M. Ernzerhof, Physical Review Letters, 1996, **77** (18), 3865-3868.
61. J. P. Perdew, J. A. Chevary, S. H. Vosko, K. A. Jackson, M. R. Pederson, D. J. Singh and C. Fiolhais, Physical Review B, 1992, **46** (11), 6671-6687.
62. H. Jonsson, G. Mills, K. W. Jacobsen and B. J. Berne, *Classical and Quantum Dynamics in Condensed Phase Simulations*. (World Scientific, Singapore, 1998).
63. L. S. Cavalcante, M. A. P. Almeida, W. Avansi, Jr., R. L. Tranquilin, E. Longo, N. C. Batista, V. R. Mastelaro and M. Siu Li, Inorganic Chemistry, 2012, **51** (20), 10675-10687.
64. T. George, S. Joseph and S. Mathew, Pramana-Journal of Physics, 2005, **65** (5), 793-799.
65. B. Hu, L.-H. Wu, S.-J. Liu, H.-B. Yao, H.-Y. Shi, G.-P. Li and S.-H. Yu, Chemical Communications, 2010, **46** (13), 2277-2279.
66. X. Wang, S. Li, H. Yu and J. Yu, Journal of Molecular Catalysis a-Chemical, 2011, **334** (1-2), 52-59.
67. X. J. Cui, S. H. Yu, L. L. Li, L. Biao, H. B. Li, M. S. Mo and X. M. Liu, Chemistry-a European Journal, 2004, **10** (1), 218-223.
68. J. A. Faucheaux, A. L. D. Stanton and P. K. Jain, Journal of Physical Chemistry Letters, 2014, **5** (6), 976-985.
69. S. A. Maier, *Plasmonics: Fundamentals and Applications*. (Springer, New York, 2007).
70. C. F. H. Bohren, D. R., *Absorption and Scattering of Light by Small Particles*. (Wiley, New York, 1983).
71. I. Kriegel, J. Rodriguez-Fernandez, A. Wisnet, H. Zhang, C. Waurisch, A. Eychmueller, A. Dubavik, A. O. Govorov and J. Feldmann, Acs Nano, 2013, **7** (5), 4367-4377.
72. A. M. Schimpf, N. Thakkar, C. E. Gunthardt, D. J. Masiello and D. R. Gamelin, Acs Nano, 2014, **8** (1), 1065-1072.
73. P. M. Skarstad and S. Geller, Materials Research Bulletin, 1975, **10** (8), 791-799.

Physical Chemistry Chemical Physics Accepted Manuscript

This journal is © The Royal Society of Chemistry [year]